International Journal of Basic and Applied Sciences, 14 (6) (2025) 425-434

International Journal of Basic and Applied Sciences

Website: www.sciencepubco.com/index.php/IJBAS
https://doi.org/10.14419/kgcxv072
Research paper

SE-Fundusnet: A Channel Attention-Based Deep Learning Architecture for Papilledema Detection and Classification

Rajalingam Arumuganainar [1] *, Navaprakash. N. [2], G. Charulatha [2], V. Suresh Kumar [2], K. Sathish [2], M. Ramkumar Prabhu [2]

[1] Department of Engineering and Technology, University of Technology and Applied Sciences, Shinas, Sultanate of Oman
[2] Department of Electronics and Communication Engineering, Saveetha School of Engineering, Saveetha Institute of Medical and Technical Sciences, Saveetha University, Chennai, Tamil Nadu, India
**Corresponding author E-mail: ramkumarprabhu@gmail.com*

Received: July 31, 2025, Accepted: September 1, 2025, Published: October 19, 2025

Abstract

Papilledema is characterized by enlargement of the optic disc resulting from increased intracranial pressure, and represents a critical clinical finding that demands immediate medical attention. A new deep learning method for automatically identifying papilledema from fundus images is presented in this work. A Hybrid Centric convolutional neural network (HCCNN) architecture is introduced that incorporates squeeze-and-excite (SE) channel attention mechanisms and parallel feature extraction to effectively capture diagnostically relevant features. The model employs different kernel sizes across parallel processing pathways to simultaneously extract fine-grained details and broader contextual features. Experimental results demonstrate excellent performance, with an overall accuracy of 96.98%, sensitivity of 95.48% and specificity of 97.74%. Ablation studies confirm the effectiveness of the SE blocks, which improve detection accuracy by 4.3%, particularly for subtle presentations. This work represents a significant step toward developing reliable computer-aided diagnostic tools for papilledema, potentially enhancing early detection and monitoring of this vision-threatening condition.

Keywords: *Papilledema Detection; Fundus Imaging; Deep Learning; Channel Attention; Convolutional Neural Networks; Medical Imaging.*

1. Introduction

An increase in intracranial pressure that causes the optic disc (OD) to enlarge is known as papilledema, serving as a significant biomarker that may signify severe neurological disorders such as brain tumors, hemorrhages, or hydrocephalus J.S. Xie et al [1]. Elevated intracranial pressure Reier, L et al [2] is a dangerous condition that can result in blindness. There are no restricted neurological results and no evident abnormalities, other than elevated cerebrospinal fluid (CSF) levels, Kwok, J.M. et al [3]. Prompt and precise identification of papilledema is crucial for preventing irreversible vision loss and facilitating appropriate medical intervention. Fundus imaging Rambabu, L et al [4], a non-invasive and popular ophthalmic technology, offers precise visualization of the retina and optic disc, making it an effective tool for evaluating papilledema. Traditional techniques for identifying papilledema depend on manual inspection by ophthalmologists, which may be subjective, time-consuming, and susceptible to inter-observer variability. The increasing availability of digital fundus images and improvements in artificial intelligence, especially deep learning Vasseneix, C et al [5], have demonstrated significant potential for automated detection methods to enhance diagnostic accuracy and consistency.

Emerging innovations in artificial intelligence (AI) have facilitated new opportunities for automated analysis of retinal images. Convolutional neural networks, or CNNs, have demonstrated remarkable performance in various medical image classification tasks, such as diabetic retinopathy, hypertensive retinopathy, age-related macular degeneration, and glaucoma. Nevertheless, few investigations have focused on the automated categorization of papilledema and its distinction from pseudopapilledema Chen, J.J. et al [6], particularly utilizing structures designed for this specific purpose. When the pressure inside the skull rises, the optic disc swells. This is called papilledema, and it can be a sign of more serious nerve problems like brain tumors, hemorrhages, or hydrocephalus. It's very important to identify papilledema quickly and correctly, because waiting too long can cause vision loss or permanent damage to the nervous system. In contrast, pseudopapilledema is a harmless disease that looks like papilledema but doesn't cause high intracranial pressure. It could be caused by a drusen optic disc or a birth defect, and it usually doesn't need immediate treatment. The overlapping visual characteristics of papilledema and pseudopapilledema in fundus imaging necessitate accurate classification to prevent misdiagnosis. A sample image illustrating both papilledema and pseudopapilledema is presented in Figure 1.

Fig. 1: Sample Fundus Images Illustrating (A) Papilledema, Showing Optic Disc Swelling with Blurred Margins and Obscured Vessels Due to Raised Intracranial Pressure, and (B) Pseudopapilledema, Showing A Similarly Elevated Optic Disc but with Sharp Margins and No Vascular Obscuration, Commonly Caused by Optic Disc Drusen.

A unique deep learning model based on a multi-module HCCNN Latha et al [7] architecture supplemented with Squeeze-and-Excitation (SE) Üzen, H et al [8] blocks is proposed to address this gap. By employing different convolutional kernel sizes, our model can extract both low-level and high-level characteristics, allowing for strong differentiation across the Normal, Papilledema, and Pseudopapilledema classes. The SE blocks enhance diagnostically relevant characteristics by recalibrating channel-wise feature responses, hence augmenting classification accuracy.

The key contributions are summarised as follows:

- To enhance feature representation, a unique HCCNN design that consists of five module convolutional blocks, each of which incorporates SE-based channel attention, is proposed.
- Multi-scale feature extraction is achieved using convolutional layers employing various kernel sizes and feature concatenation, hence enhancing the model's ability to recognize both localized and global patterns.
- The proposed papilledema detection method is evaluated using a labeled dataset and exhibits high classification accuracy in differentiating normal cases from those of papilledema and pseudopapilledema.

The paper is organized as follows: Section 2 examines the relevant research on automated papilledema detection. Section 3 provides a comprehensive explanation of the proposed approach. The experimental design, findings, and their discussion are presented in Section 4. The conclusions of the research are presented in Section 5.

2. Literature Review

Detection of papilledema is essential for recognizing high intracranial pressure (ICP) and preventing vision impairment. Recent improvements in clinical and technological methodologies have improved the precision and efficacy of papilledema diagnosis. Detection of papilledema involves assessing edema at the optic nerve head resulting from elevated intracranial pressure. Kokulu et al. [9] employed transfer learning on color fundus images, attaining a high accuracy of 0.96 using MobileNetV2, and improved detection by histogram equalization and 3D box filtering. Avramidis et al. [10] introduce a deep learning model for the automated detection of pediatric papilledema, employing optic disc localization and explainable indicators, achieving diagnostic accuracy comparable to expert ophthalmologists, thereby improving clinical diagnosis and management of this condition.

Saba et al. [11] introduce an automated approach utilizing deep learning to detect and grade papilledema utilizing U-Net and Dense-Net designs. This methodology comprises two primary phases. In the retinal images, the OD and the area next to it are found and cropped so that they can be fed into Dense-Net. This network decides whether the OD is normal or has papilledema. After being categorized, the Dense-Net-identified papilledema images are preprocessed with Gabor filtering. The images that have been processed are then sent to the U-Net for vascular network segmentation to grade papilledema.

An automated technique, Akbar, S et al [12], is introduced that identifies and evaluates papilledema by analyzing fundus retinal pictures. This methodology extracts a total of 23 features, comprising six textural characteristics obtained from the Gray-Level Co-occurrence Matrix (GLCM), eight parameters associated with optic disc margin obscuration, three color-derived features, and seven vascular attributes. A feature vector comprising these attributes is employed for the categorization of normal and papilledema images via a Support Vector Machine (SVM). The suggested approach demonstrates an overall accuracy of 92.86% in classifying papilledema.

Salaheldin et al. [13] emphasize the use of innovative models for detecting papilledema, differentiating it from normal and pseudopapilledema cases, through the implementation of CNNs and recurrent neural networks (RNNs). The multi-path CNN architecture employs feature extraction to precisely detect critical papilledema indicators, and the cascaded model, which combines ResNet-50 and LSTM, proficiently catches sequential data.

Wiharto et al. [14] proposed the Squeeze-Excitation Half U-Net model, which integrates a squeeze-and-excitation mechanism to apply channel-wise attention to feature maps. The model was combined with the SMOTE to address class imbalance, achieving an accuracy of 95.89%.

Papilledema from fundus images could be automatically detected using a new computer-aided approach, Üzen, H et al [15]. Four categories of 26 features are obtained overall to find abnormalities in the optic disc caused by papilledema. After key features are identified and merged into a feature matrix, supervised Support Vector Machine (SVM) classification is performed to differentiate between normal and papilledema cases

The existing research on papilledema identification illustrates the effectiveness of deep learning and image processing methods in recognizing optic disc swelling from fundus images. Multiple approaches have employed transfer learning models such as MobileNetV2, handcrafted features, and segmentation-based methods to identify papilledema with significant precision. However, these methodologies encounter numerous constraints, including heavy reliance on preprocessing, complex multi-stage pipelines, restricted capacity to distinguish pseudopapilledema from real papilledema, and inadequate model interpretability. The proposed CA-HCCNN addresses some of the issues with existing approaches by making pre-processing easier than U-Net-based methods and using SE-based channel attention to improve feature discrimination. This approach improves classification accuracy while remaining computationally efficient.

3. Methodology

3.1. Overview

A novel deep learning method for the automatic identification of papilledema from retinal fundus images is presented in this work. Squeeze-and-Excite (SE) channel attention mechanism, which dynamically recalibrates feature maps by prioritizing important features and suppressing less relevant ones, are carefully incorporated into the model architecture as depicted in Fig. 2. Additionally, the method makes use of domain-specific data augmentation methods that are suited to the properties of fundus images, including rotation, flipping, intensity normalization, and contrast enhancement, to strengthen the model's resilience to variations in retinal imaging and its capacity for generalization.

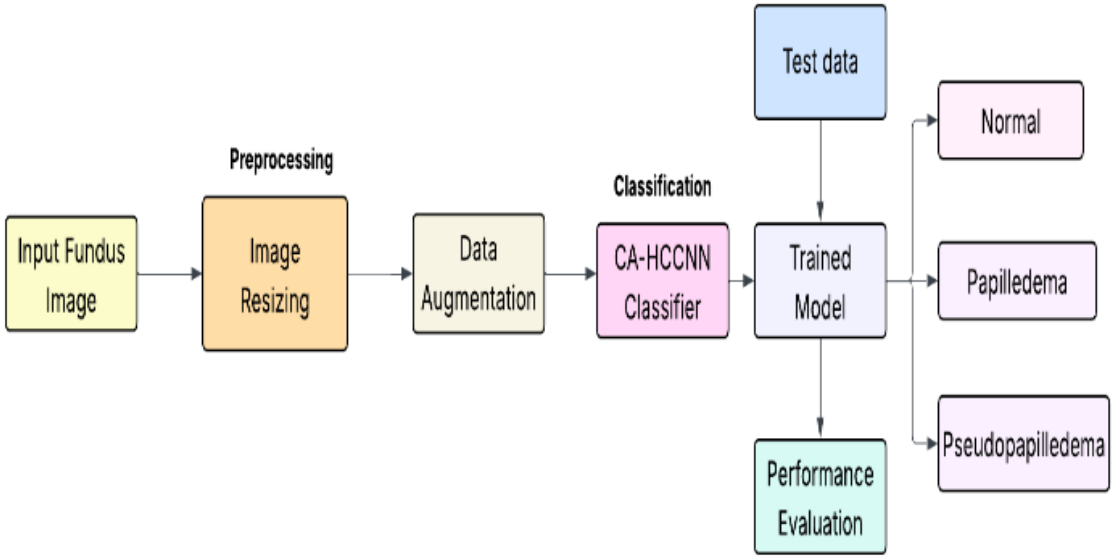

Fig. 2: Schematic Representation of the Proposed Approach for Papilledema Detection.

3.2. Dataset preparation

Fundus images were acquired and classified into three categories: normal, papilledema, and pseudopapilledema Kim, U et al [17]. The dataset is divided into 70% for model training, 15% for testing evaluation, and 15% for validation assessment. All images were standardized to 224×224 pixels to ensure consistent input dimensions for the neural network. The dataset comprised 280 photos obtained from KK Hospital, guaranteeing a proportional representation of papilledema, pseudopapilledema, and normal patients. It includes patient demographics (males: 26–68 years, females: 23–56 years) and differences in image quality to make the proposed method more generalizable and to show how different groups of people can be included.

3.2.1. Dataset balancing

A systematic oversampling technique Huda, S et al [18]) was used to rectify the class imbalance present in our dataset. Class imbalance is a serious problem in medical image classification tasks because it can cause models to be biased towards majority classes and reduce the sensitivity of diagnosis for illnesses that are not well represented. High sensitivity is clinically necessary for the identification of papilledema; hence, this is especially challenging. This balancing approach utilized direct image duplication followed by augmentation. Algorithm 1 outlines the implementation of the balancing strategy:

Algorithm 1: Dataset Balancing via Oversampling

Input: Original dataset with class imbalance
Output: Balanced dataset with equal class representation 1. Identify the quantity of images in each category. 2. Determine the majority class count (target count) 3. For each class: a. Create a corresponding directory in the balanced dataset b. Copy all original images to the balanced directory c. Calculate additional images needed: target count - current count d. Randomly select and duplicate images from the class until reaching the target count 4. Apply fundus-specific augmentation during training

The algorithm initially examines the class distribution in the original dataset, selecting the majority class as the goal count for all classes. Each minority class is augmented by randomly duplicating existing samples until all classes possess an equal quantity of images. In order to maintain the genuine feature distribution within each category, it is essential to keep all of the original images. This method produced a balanced dataset with 779 images per class instead of the initial unbalanced distribution, where papilledema cases were outnumbered by normal images.

To mitigate potential overfitting caused by duplicate images, we enhanced this static balance with dynamic augmentation like rotation (±15°), horizontal/vertical shifts (10% of image dimensions), horizontal flipping, and zooming during model training, utilizing the Image Data Generator Awaluddin, B.A et al [19]. This combination of static duplication and dynamic augmentation guaranteed that the model encountered an equal number of samples from each class, while maintaining substantial feature selection through transformational variations. The balanced dataset, as in Fig. 3, substantially enhanced model performance, especially with sensitivity measures in the papilledema category.

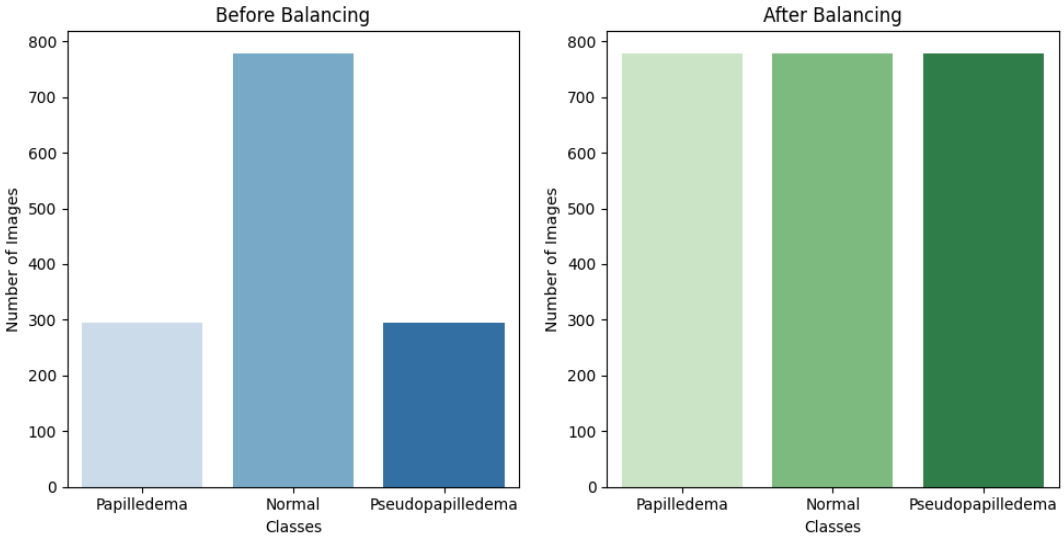

Fig. 3: Description of the Dataset before and after Balancing.

3.3. Model architecture

Multiple parallel processing paths and channel attention techniques were incorporated into the hybrid centric convolutional neural network (HCCNN) [7] that was built. Both fine-grained features and broader complex features that are essential for papilledema diagnosis were taken into consideration during the design process of the architecture.

3.3.1. Channel attention mechanism

The squeeze-and-excite (SE) block Wang, K et al [20], which is known for its implementation of channel attention, is the fundamental component of our system, as shown in Fig. 4. The channel-wise feature responses are adaptively recalibrated by this mechanism, which does so by:

1) Squeeze Operation: Aggregating feature maps across spatial dimensions through the use of global average pooling is the first step in the squeeze operation algorithm.

$$X_c = \frac{1}{Hxw}\sum_{i=1}^{H}\sum_{j=1}^{W} x_c(i,j)$$

2) Excitation Operation: Utilizing a two-layer fully linked network that incorporates dimensionality reduction and expansion to obtain channel-specific weights.

$$s = \sigma(W_2\delta(W_1 z))$$

3) Recalibration of Features: The process of applying these weights to the initial feature maps through the use of channel-wise multiplication.

$$\widetilde{X_c} = s_c . X_c$$

Where δ refer to the ReLU function, σ denotes the sigmoid function, and W_1 and W_2 are the dimensionality-reduction and dimensionality-expansion layer parameters, respectively.

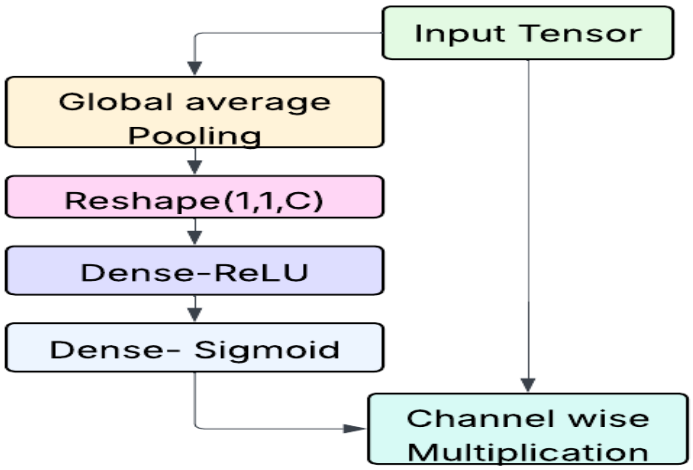

Fig. 4: Squeeze and Excitation Block.

3.3.2. HCCNN network architecture

HCCNN consists of five primary modules with different kernel sizes to capture multi-scale features, as shown in the Figure:

1) Module 1: 5×5 convolution, ReLU activation, SE block, and 2×2 max pooling
2) Module 2: 3x3 convolution, ReLU activation, SE block, and 2×2 max pooling
3) Module 3: 7×7 convolution, ReLU activation, SE block, and 2×2 max pooling
4) Module 4: 5×5 convolution, ReLU activation, SE block, and 2×2 max pooling
5) Module 5: 3×3 convolution, ReLU activation, SE block, and 2×2 max pooling

The information flow has multiple paths, which is a noteworthy feature of this architecture. The initial input image is processed by both Module 1 and Module 3, each having its own unique receptive fields. The output of Module 3 is then fed into Module 4. For the purpose of forming the input for Module 5, the outputs from Modules 1 and 3 are combined. Finally, outputs from Modules 3, 4, and 5 are combined before classification layers as shown in Fig. 5. This structure creates multiple information pathways with varying depths, allowing the network to simultaneously extract and integrate features at different levels of abstraction.

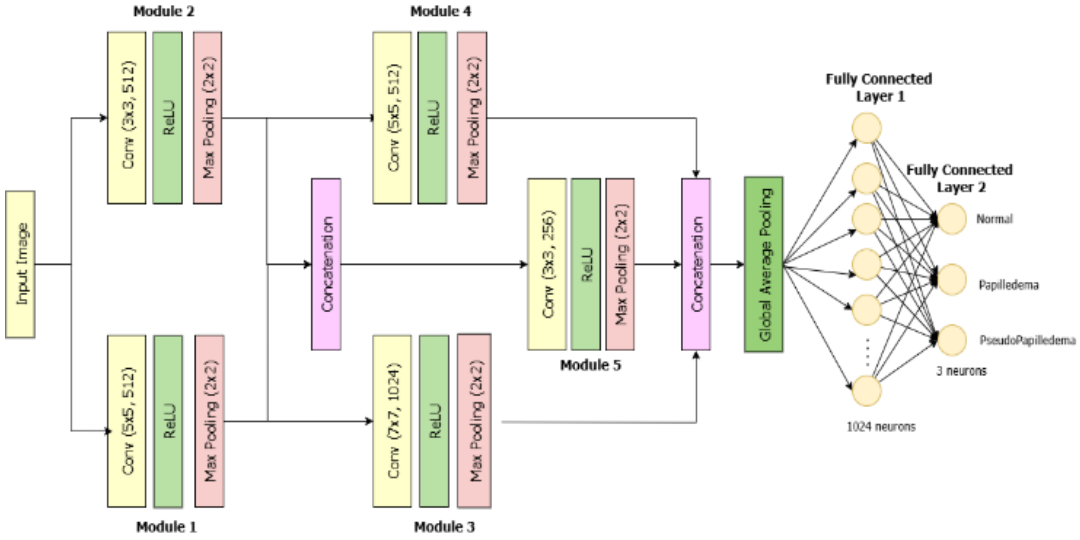

Fig. 5: HCCNN Architecture.

The feature maps obtained from the concatenated paths are subjected to an extra layer called the Global Average Pooling (GAP) layer, Kumar, R.L et al [21]. The primary role of the Global Average Pooling (GAP) layer is to reduce the spatial dimensions (height and width) of the feature maps, while retaining essential information across the depth (channels). This is accomplished by reducing the size of the feature maps. The GAP layer, in contrast to standard flattening, which results in a greater number of parameters, significantly reduces complexity and improves generalization by computing the average of each feature map. During this process, the multidimensional features are converted into a compact one-dimensional vector, with each value representing a summarised response of the feature channel that corresponds to it. Two fully connected layers follow this:

- A hidden layer consisting of 1024 neurons, utilizing the ReLU activation function.
- An output layer with 3 units and softmax activation for final classification

The ReLu and Softmax, Chopade et al [22] activation is defined by, The ReLU activation function introduces nonlinearity to the network, enabling it to identify intricate relationships. Conversely, Softmax produces normalized probability scores for the three classes, enhancing the interpretability of the results.

$$\mathrm{ReLu}(x) = \max(0, x)$$

$$\mathrm{softmax}(z_i) = \frac{e^{z_i}}{\sum_{j=1}^{n} e^{z_j}}$$

Where z_i denotes the i^{th} element of the vector, and the denominator sums over all elements.

3.3.3. Proposed CA-HCCNN model

The proposed model utilizes a multi-scale feature extraction approach by incorporating parallel convolutional layers with diverse kernel sizes (3×3, 5×5, and 7×7), allowing it to effectively capture both fine and coarse features essential for differentiating subtle differences between papilledema and pseudopapilledema. To increase the discriminative capability of the network, Squeeze-and-Excitation (SE) blocks are incorporated into each module, providing channel-wise attention through the adaptive recalibration of feature responses according to their significance. The architecture employs efficient fusion by strategically concatenating intermediate feature maps, enhancing feature integration without substantial computational expense. Both accuracy and efficiency in papilledema classification tasks are guaranteed by the model's end-to-end training and compactness despite its multi-branch design. Figure 6 shows the proposed CA-HCCNN model architecture.

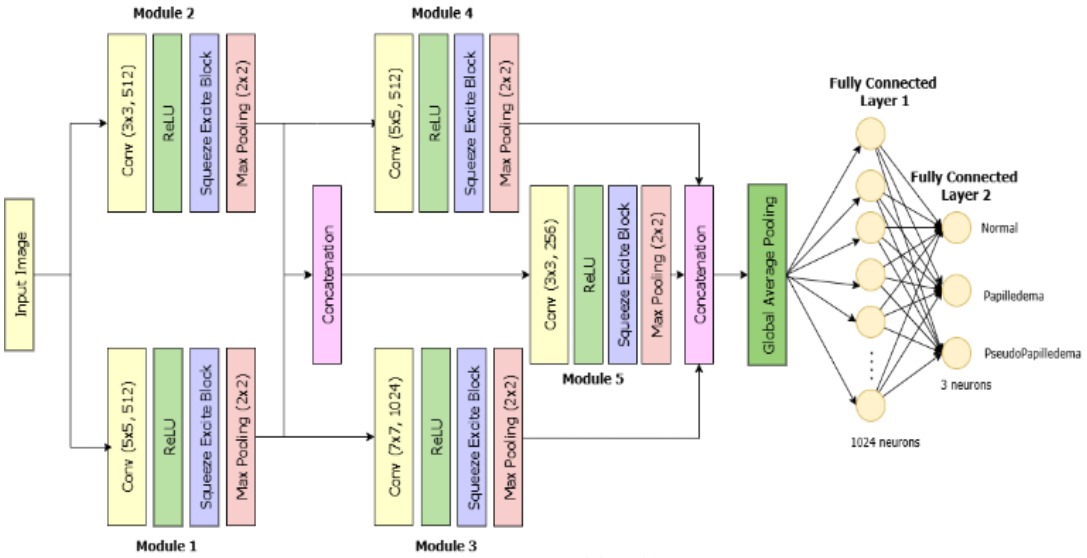

Fig. 6: CA-HCCNN Model Architecture.

The proposed CA-HCCNN model was trained using a carefully chosen set of hyperparameters to improve learning performance and avoid overfitting. Table 1 highlights key hyperparameters employed during training. In order to make sure the model was stable and converged, these parameters were improved empirically using cross-validation and several iterations. The selected configuration allowed the CA-HCCNN to learn appropriate features from fundus images to correctly classify cases of papilledema, pseudopapilledema, and normal.

Table 1: Hyperparameters Used in SE-HCCNN

Parameter	Configuration
Number of Epochs	50
Batch Size	32
Input Dimension	224x224
Optimizer	Adam
Loss Function	Categorical Cross-Entropy
Learning rate	0.001
Dropout rate	0.5

3.4. Implementation details

The retinal disorder classification model, CA-HCCNN, was created using Python 3.7 and implemented on the Google Colab platform, which provides resources for computationally difficult applications. An NVIDIA T4 graphics processing unit with 16 gigabytes of RAM was used to speed up the model's activities. This hardware setup offered the processing capacity required to effectively train and operate the complex neural network design. The Adam optimizer was used with an initial learning rate of 0.01, and categorical cross-entropy was selected as the loss function. Model training was conducted using a batch size of 32 images. The ImageDataGenerator class was utilized to process training and validation data, with real-time augmentation exclusively applied to the training set. The validation set was just rescaled to standardize pixel values within the range of 0 to 1.

4. Results and discussion

4.1. Model performance metrics

The squeeze-and-excite channel attention-based HCCNN attained excellent outcomes in the automatic identification of papilledema from fundus images. The model was assessed using a variety of performance metrics [23] in order to guarantee a thorough evaluation.

$$\text{Accuracy} = \frac{TP+TN}{TP+FN+TN+FP}$$

$$\text{Sensitivity(Recall)} = \frac{TP}{TP+FN}$$

$$\text{Specificity} = \frac{TN}{TN+FP}$$

$$\text{Precision} = \frac{TP}{TP+FP}$$

$$\text{F1Score} = 2\frac{(\text{Precision} * \text{Recall})}{(\text{Precision}+\text{Recall})}$$

Fig 7 presents the confusion matrices of the CA-HCCNN model on the test set before and after dataset balancing. Before balancing, the model exhibited a bias towards the majority class, incorrectly identifying numerous cases of papilledema and pseudopapilledema. Following the implementation of dataset balance, classification performance exhibited improvement across all categories, with a notable decrease in false negatives and higher detection of minority classes, signifying increased model dependability and generalization.

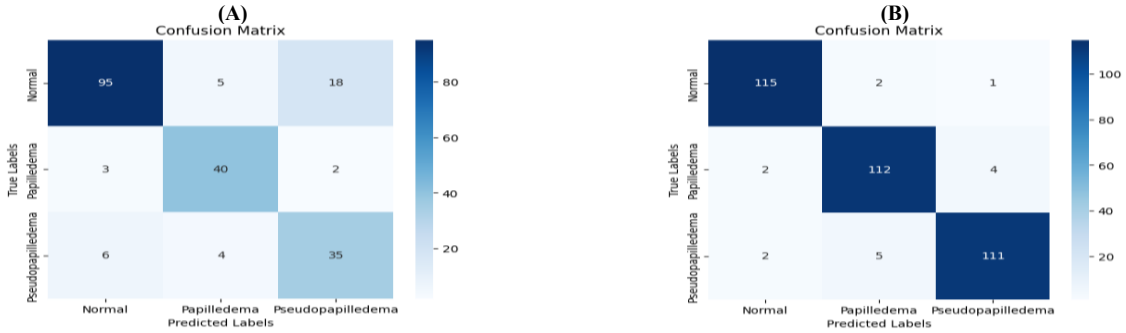

Fig. 7: Confusion Matrices Showing Classification Performance (A) before Dataset Balancing and (B) After Dataset Balancing. After Balancing, the Model Demonstrates Significantly Fewer False Negatives in Papilledema Detection, Highlighting Improved Reliability.

4.2. Performance before dataset balancing

Initial training on the imbalanced dataset resulted in skewed performance since the model was exposed to more samples from the majority class (Normal) than the minority classes (Papilledema and Pseudopapilledema). Table 2 displays the performance characteristics of the CA-HCCNN model prior to the implementation of any dataset balancing methods. The findings demonstrate that the model's accuracy, sensitivity, and specificity exhibited bias towards the majority class, highlighting the influence of class imbalance on classification performance.

Table 2: Performance Metrics Before Dataset Balancing

Class	Accuracy (%)	Sensitivity (%)	Specificity (%)	Precision (%)	F1 score (%)
Normal	84.62	80.51	90	91.35	85.59
Papilledema	93.27	88.89	94.48	81.63	85.11
Pseudopapilledema	85.58	77.78	87.73	63.64	70
Average	87.82	82.39	90.73	78.87	80.23

The overall accuracy on the imbalanced test set was 87.82%. However, the model shows Malla et al [23] a strong overall performance, particularly for Papilledema detection, with high accuracy and sensitivity. However, Pseudopapilledema classification is comparatively weaker, indicating a need for further refinement or data balancing.

4.3. Performance after dataset balancing

Training on the balanced dataset significantly improved model performance, particularly for the papilledema class. Table 3 presents the performance metrics after implementing the balancing strategies:

Table 3: Performance Metrics after Dataset Balancing

Class	Accuracy (%)	Sensitivity (%)	Specificity (%)	Precision (%)	F1 score (%)
Normal	98.02	97.46	98.31	96.64	97.05
Papilledema	96.33	94.92	97.03	94.12	94.51
Pseudopapilledema	96.61	94.07	97.88	95.69	94.87
Average	96.98	95.48	97.74	95.48	95.47

The overall accuracy improved to 96.98% representing a 9% absolute increase. The model performs exceptionally well in all three classes, exhibiting high sensitivity, specificity, and accuracy. Reliable classification is indicated by the consistent precision and F1 scores, especially when it comes to accurately recognizing difficult cases like papilledema and pseudopapilledema. The figure illustrates the confusion matrices of the proposed CA-HCCNN model before and after dataset balancing, highlighting the reduction in misclassifications.

4.4. ROC analysis

The Receiver Operating Characteristic (ROC) curve, Saenz, R et al[24], illustrates the efficacy of our model in distinguishing among three categories of fundus images: Normal, Papilledema, and Pseudopapilledema. The high AUC ratings (0.94 for Normal, 0.97 for Papilledema, and 0.91 for Pseudopapilledema) indicate that the model excels in differentiating across these categories. It excels in identifying papilledema, the most severe of the three diseases. The steep rise of the papilledema curve (depicted in orange) indicates that the model identifies the majority of cases with minimal false positives, rendering it effective for early detection. As seen in the Figure, the model preserved high sensitivity without significantly affecting specificity.

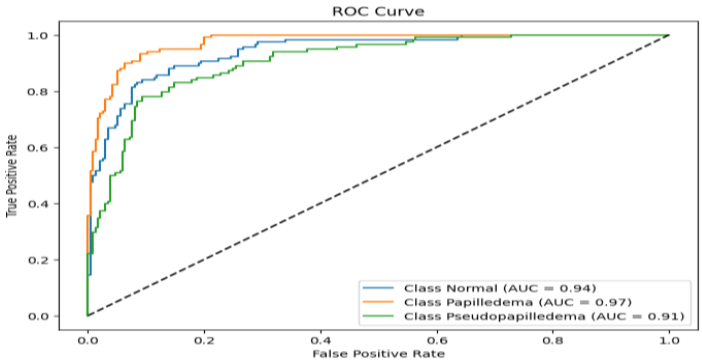

Fig. 8: ROC Curve.

4.5. Model performance analysis

Table 4 provides a comparative analysis between the proposed HCCNN and CA-HCCNN models, focusing on the number of trainable parameters, training and validation accuracies, as well as their respective loss values. The HCCNN model, comprising around 36.496 million parameters, achieved training and validation accuracies of 92.56% and 90.35%, respectively, with corresponding loss values of 0.21 for training and 0.29 for validation. Conversely, the CA-HCCNN model, which integrates Channel Attention (CA) mechanisms via Squeeze-and-Excitation (SE) blocks, exhibits a marginally increased parameter count of 36.734 million. This enhancement leads to significant performance gains, yielding training accuracy of 97.42% and validation accuracy of 96.58%. The associated training and validation losses are markedly reduced, at 0.15 and 0.16, respectively. This highlights the importance of integrating channel attention modules, which enhance the model's capacity to concentrate on salient features, thus enhancing generalization and mitigating overfitting. The CA-HCCNN outperforms the baseline HCCNN in all m, indicating its effectiveness for precise papilledema classification from fundus images.

Table 4: Performance Comparison of HCCNN and CA-HCCNN Models

Model	No. of parameters	Training accuracy (%)	Validation accuracy (%)	Training Loss	Validation Loss
HCCNN	36.496 million	92.56%	90.35	0.21	0.29
CA-HCCNN	36.734 million	98.42%	96.58	0.15	0.16

4.6. Ablation studies

An ablation study was carried out to assess the effects of the Channel Attention (CA) mechanism incorporated into the proposed HCCNN model. To differentiate between the Normal, Papilledema, and Pseudopapilledema classes, the CA blocks—which are implemented using Squeeze-and-Excitation (SE) modules—were to be isolated and their contribution to the total classification performance quantified. For comparison, two model variations were developed:

a) The initial hybrid centric CNN architecture without an attention mechanism is known as the baseline HCCNN.
b) The improved CA-HCCNN version adds SE-based channel attention blocks following each convolutional module.

Table 5: Ablation Study

Model	Sensitivity (%)	Specificity (%)	Precision (%)	F1 score (%)	Accuracy (%)
HCCNN	88.98	94.49	88.98	88.97	92.65
CA-HCCNN (Proposed Method)	95.48	97.74	95.48	95.47	96.98

The elimination of the SE blocks from the model architecture led to a significant decrease in classification performance, specifically a 4.3% fall in total accuracy. This underscores the importance of channel-wise attention methods introduced by SE blocks, which enable the model to prioritize the most useful characteristics across channels.

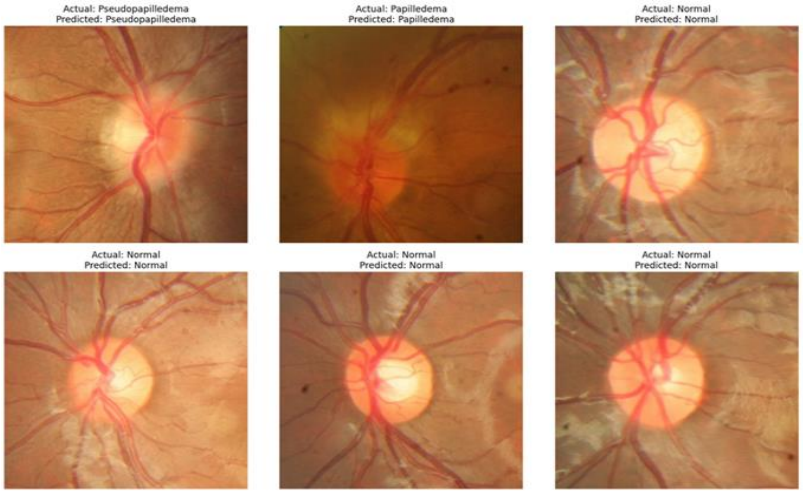

Fig. 9: Classification Output of CA-HCCNN Model.

4.7. Visualization of model attention

Gradient-weighted Class Activation Mapping (Grad-CAM) Szanto, D et al [25] was utilized to visualize areas of interest that impacted the model's conclusions. The figure displays activation heatmaps superimposed on original fundus pictures. In cases of papilledema, the model constantly concentrated on the optic disc region, emphasizing disc borders, vascular patterns, and peripapillary areas, in accordance with clinical diagnostic criteria. Under typical circumstances, attention was more uniformly distributed over the optic disc, without particular focus on the characteristics linked to papilledema.

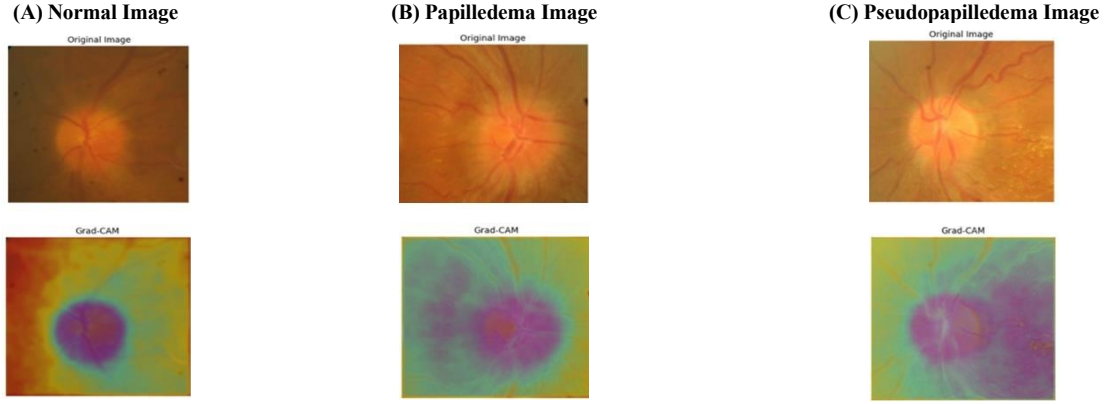

Fig. 10: Grad CAM Visualization of CA-HCCNN.

Table 6: Comparative Performance Evaluation of the Proposed Method with Existing Techniques

Study	Sensitivity (%)	Specificity (%)	Precision (%)	F1 score (%)	Accuracy (%)
Akbar et al. [26]	90.01	96.39	--	--	92.86
Fathima et al. [27]	83.94	88.39	--	--	85.89
Oumarou et al. [28]	54.12	--	55.2	55.17	53.61
Biousse et al. [29]	84	89.6	--	--	--
Yang et al. [30]	94.3	95.7	--	--	95.1
HCCNN [15]	88.98	94.49	88.98	88.97	92.65
CA-HCCNN (Proposed)	95.48	97.74	95.48	95.47	96.98

The comparative analysis in Table 6 reveals that the proposed CA-HCCNN model significantly outperforms existing methods across all performance metrics. Most notably, CA-HCCNN achieves a 96.98% accuracy, which represents a substantial improvement over previous state-of-the-art methods, including Yang et al. (95.1%) and the baseline HCCNN model (92.65%). The enhanced performance is particularly evident in sensitivity (95.48%) and specificity (97.74%), indicating the model's superior capability in both detecting papilledema cases and avoiding false positives. This enhancement is primarily due to the incorporation of channel attention mechanisms, which allow the model to concentrate on the most relevant and discriminative features for accurate papilledema detection.

5. Conclusion

The proposed channel attention-based HCCNN demonstrates promising performance for automated papilledema detection from fundus images. The architectural innovations, particularly the squeeze-and-excite blocks and parallel feature extraction, contribute significantly to the model's effectiveness. Experimental findings indicate outstanding performance, with an overall accuracy of 96.98%, sensitivity of 95.48%, and specificity of 97.74%. Ablation experiments validate the efficiency of the SE blocks, enhancing detection accuracy by 4.3%, especially for subtle presentations. This study marks a substantial advancement in the creation of dependable computer-aided diagnostic instruments for papilledema, potentially improving early identification and surveillance of this vision-impairing disorder. Our results suggest that deep learning approaches can provide valuable decision support for ophthalmologists and neurologists in the diagnosis of papilledema, potentially improving efficiency and consistency in clinical practice.

Limitations of SE-FundusNet include significant computational demands that may impede its implementation in resource-constrained settings, the need for additional validation on images of exceptionally low quality, and the opportunity to increase dataset diversity through multi-institutional contributions to improve generalisability. Future efforts will primarily concentrate on integrating SE-FundusNet with optical coherence tomography (OCT) for multimodal diagnostics, creating lightweight variations for real-time clinical applications, and investigating integration with electronic health record (EHR) systems to enable seamless clinical processes.

References

[1] J.S. Xie, L. Donaldson, E. Margolin, Papilledema: a review of etiology, pathophysiology, diagnosis, and management, Surv. Ophthalmol. 67 (2022) 1135–1159. https://doi.org/10.1016/j.survophthal.2021.11.007.

[2] Reier, L., Fowler, J.B., Arshad, M., Hadi, H., Whitney, E., Farmah, A.V. and Siddiqi, J., 2022. Optic disc edema and elevated intracranial pressure (ICP): a comprehensive review of papilledema. Cureus, 14(5). https://doi.org/10.7759/cureus.24915.

[3] Kwok, J.M., Mandell, D.M. and Margolin, E.A., 2021. Papilledema in a patient with intracranial hypotension. Journal of Neuro-Ophthalmology, 41(4), pp. e708-e710. https://doi.org/10.1097/WNO.0000000000001112.

[4] Rambabu, L., Edmiston, T., Smith, B.G., Kohler, K., Kolias, A.G., Bethelehem, R.A., Keane, P.A., Marcus, H.J., Hutchinson, P.J. and Bashford, T., 2025. Detecting papilloedema as a marker of raised intracranial pressure using artificial intelligence: a systematic review. medRxiv, pp.2025-02. https://doi.org/10.1101/2025.02.14.25322289.

[5] Sathish, K., 2025, February. Investigation of Impedance Tube-based Parameter Estimation Techniques with Data Generation for Underwater Acoustic Applications. In 2025 International Conference on Electronics and Renewable Systems (ICEARS) (pp. 154-159). IEEE. https://doi.org/10.1109/ICEARS64219.2025.10940315.

[6] Prabhu, M., Sathishkumar, A., Sasi, G., ... Lau Chee Yong, Shanker, M.C., Selvakumarasamy K, "Monkeypox Detection using CSA based K-Means Clustering with Swin Transformer Model", Journal of Machine and Computing, 4(2), pp. 400–407 (2024). https://doi.org/10.53759/7669/jmc202404038.

[7] Latha, G., Priya, P.A. & Smitha, V.K. Enhanced diabetic retinopathy detection and exudates segmentation using deep learning: A promising approach for early disease diagnosis. Multimedia Tools and Applications 83, 77785–77808 (2024). https://doi.org/10.1007/s11042-024-18629-7.

[8] Üzen, H., Turkoglu, M., Aslan, M. and Hanbay, D., 2023. Depth-wise Squeeze and Excitation Block-based Efficient-Unet model for surface defect detection. The Visual Computer, 39(5), pp.1745-1764. https://doi.org/10.1007/s00371-022-02442-0.

[9] Kokulu, M. and Göker, H., 2023. Detection of papilledema severity from color fundus images using transfer learning approaches. https://doi.org/10.29002/asujse.1280766.

[10] Avramidis, K., Rostami, M., Chang, M. Y., & Narayanan, S. S. (2022). Automating Detection of Papilledema in Pediatric Fundus Images with Explainable Machine Learning. International Conference on Information Photonics, 3973–3977. https://doi.org/10.1109/ICIP46576.2022.9897529.
[11] Saba, T., Akbar, S., Kolivand, H., Kolivand, H., & Bahaj, S. A. (2021). Automatic detection of papilledema through fundus retinal images using deep learning. Microscopy Research and Technique, 84(12), 3066–3077. https://doi.org/10.1002/jemt.23865.
[12] Akbar, S., Akram, M. U., Sharif, M., Tariq, A., & Yasin, U. U. (2017). Decision Support System for Detection of Papilledema through Fundus Retinal Images. Journal of Medical Systems, 41(4), 1–16. https://doi.org/10.1007/s10916-017-0712-9.
[13] Salaheldin, A. M., Abdel Wahed, M., Talaat, M., & Saleh, N. (n.d.). An evaluation of AI-based methods for papilledema detection in retinal fundus images. Biomedical Signal Processing and Control. https://doi.org/10.1016/j.bspc.2024.106120.
[14] Wiharto, A.E.P.S., Squeeze-excitation half U-Net and synthetic minority oversampling technique oversampling for papilledema image classification. Int J Artif Intell ISSN, 2252(8938), p.1411.
[15] Fatima, K.N., Hassan, T., Akram, M.U., Akhtar, M. and Butt, W.H., 2017. Fully automated diagnosis of papilledema through robust extraction of vascular patterns and ocular pathology from fundus photographs. Biomedical optics express, 8(2), pp.1005-1024. https://doi.org/10.1364/BOE.8.001005.
[16] Kapileswar, N., 2025, June. Federated Deep Learning-Driven Cloud-IoT Framework for Real-Time Healthcare Monitoring and Privacy-Preserving Anomaly Detection. In 2025 3rd International Conference on Self Sustainable Artificial Intelligence Systems (ICSSAS) (pp. 1866-1871). IEEE. https://doi.org/10.1109/ICSSAS66150.2025.11080854.
[17] Kim, U. (2018, August 1). Machine learning for Pseudopapilledema.
[18] Huda, S., Liu, K., Abdelrazek, M., Ibrahim, A., Alyahya, S., Al-Dossari, H. and Ahmad, S., 2018. An ensemble oversampling model for class imbalance problem in software defect prediction. IEEE access, 6, pp.24184-24195. https://doi.org/10.1109/ACCESS.2018.2817572.
[19] Maniraj, S.P., Rose, J.D., Arunachalam, R., K Rangasamy,, Vishal P P & Selvakumarasamy K, "Polar Region Climate Dynamics: Deep Learning and Remote Sensing Integration for Monitoring Arctic and Antarctic Changes. Remote Sens Earth Syst Sci 7, 582–595 (2024). https://doi.org/10.1007/s41976-024-00147-7.
[20] N. Kapileswar et al, "DeepCurrent: An Attention-Driven Graph Neural Network for Energy-Efficient Routing and Data Aggregation in UIoT Networks," 2025 International Conference on Modern Sustainable Systems (CMSS), Shah Alam, Malaysia, 2025, pp. 716-720, doi: 10.1109/CMSS66566.2025.11182394.
[21] Wang, K., Jiang, P., Meng, J. and Jiang, X., 2022. Attention-based DenseNet for pneumonia classification. Irbm, 43(5), pp.479-485. https://doi.org/10.1016/j.irbm.2021.12.004.
[22] Kumar, R.L., Kakarla, J., Isunuri, B.V. and Singh, M., 2021. Multi-class brain tumor classification using residual network and global average pooling. Multimedia Tools and Applications, 80(9), pp.13429-13438. https://doi.org/10.1007/s11042-020-10335-4.
[23] Chopade, P.B., Kota, P.N., Jadhav, B.D., Ghate, P.M. and Kulkarni, S.S., 2025. Retinopathy Disease Detection and Classification Using a Coordinate Attention Module-Based Convolutional Neural Network with Leaky Rectified Linear Unit. IIUM Engineering Journal, 26(1), pp.129-147. https://doi.org/10.31436/iiumej.v26i1.3194.
[24] J. Simon et al, "Dual-Branch GAN-Driven Super-Resolution for Low-Dose CT Image Enhancement under Radiological Noise Constraints," 2025 International Conference on Modern Sustainable Systems (CMSS), Shah Alam, Malaysia, 2025, pp. 710-715, doi: 10.1109/CMSS66566.2025.11182514
[25] Malla, P.P., Sahu, S. and Alutaibi, A.I., 2023. Classification of tumor in brain MR images using deep convolutional neural network and global average pooling. Processes, 11(3), p.679. https://doi.org/10.3390/pr11030679.
[26] D. Sheela, N. P. G. Bhavani, C. Prameeladevi and Ch. Sarada Devi, "Linear Tapered Wavelength Division Multiplexing (WDM) Phasor Array to Improve Coupling Efficiency," Proc. of 6th Int. Conf. on 2025 Devices for Integrated Circuit Devices, pp. 203–208, 2025. https://doi.org/10.1109/DevIC63749.2025.11012459.
[27] Szanto, D., Erekat, A., Woods, B., Wang, J.K., Garvin, M., Johnson, B.A., Kardon, R., Linton, E. and Kupersmith, M.J., 2025. Deep Learning Approach Readily Differentiates Papilledema, NAION, and Healthy Eyes. American Journal of Ophthalmology. https://doi.org/10.1016/j.ajo.2025.05.036.